Reaction dynamics of chlorine atom with methane: Dual-level *ab initio* analytic potential energy surface and isotope effects

Hua-Gen Yu and Gunnar Nyman[a)]
Department of Chemistry, Physical Chemistry, Göteborg University, S-412 96 Göteborg, Sweden

(Received 18 May 1999; accepted 27 July 1999)

An analytic potential energy surface for the $Cl+CH_4 \rightleftharpoons HCl+CH_3$ reaction in C_{3V} symmetry has been obtained by fitting to 1136 energy points from a dual-level MP2/SAC (Møller–Plesset second order perturbation/scaling all correlation) calculation using the 6-311G$(2d,d,p)$ basis set. A zero-point energy correction is made to account for all modes not explicitly treated with the time-independent quantum scattering rotating line umbrella (RLU) model, which is used for the dynamics calculations. The effective potential gives a vibrationally adiabatic ground-state barrier height of 3.36 kcal/mol and an endothermicity (0 K) of 1.19 kcal/mol for the $Cl+CH_4$ reaction, and 4.43 kcal/mol and 2.29 kcal/mol, respectively, for $Cl+CD_4$. Thermal rate constants, tunneling and kinetic isotope effects have been investigated in detail. Calculated differential cross sections for $Cl+CD_4 \rightarrow DCl+CD_3$, with reactants and products in their vibrational ground states, show that the DCl product is strongly backward scattered. Further, ground state $Cl+CD_4$ reacts to give the CD_3 product predominantly unexcited at collision energies ranging from 0.15 eV to 0.25 eV. Generally, good agreement with experimental measurements and previous theoretical work is obtained.
 [S0021-9606(99)30439-6]

I. INTRODUCTION

The reaction of a chlorine atom with methane is an important step in the Cl/O_3 destruction chain mechanism in the stratosphere. Thermal rate constants have been measured in the temperature range 200–500 K.[1] The reaction is characterized by a nonlinear Arrhenius behavior for the temperature dependence of the absolute thermal rate constants with a small activation energy (2.7–3.5 kcal/mol). The reaction has received substantial theoretical attention including several high level *ab initio* calculations[2,3] and various transition state theory calculations.[2,4–6] For the reverse reaction $HCl+CH_3 \rightarrow Cl+CH_4$, there also exist several experimental and theoretical studies.[7–10]

Recently, we have calculated rate constants, tunneling effects, product distributions and differential cross sections for the reaction of Cl with CH_4 using reduced dimensionality (2D−4D) quantum scattering models.[11–13] A pronounced tunneling effect has been obtained. From the temperature $T=200$ K to $T=800$ K, it was predicted that the ground-state tunneling coefficients vary from 14 to 2. The calculated thermal rate constants are in good agreement with the experimental results over the temperature range 200–800 K, although the theoretical values are up to 45% smaller.[11,13] It was found that vibrational excitation of CH_4 can enhance the reaction, which was first noticed by Duncan and Truong[4] and was also verified by experiments.[14] In particular, we have made more detailed studies of the state-to-state differential cross section and vibrational and rotational distributions of the CH_3 product for the ground-state and vibrationally excited CH_4 reagent in order to illustrate the experimental measurements.[14–17] For the differential cross section, qualitatively good agreement between the experimental results and our calculations has been achieved. There is, however, a discrepancy in the vibrational distribution of the umbrella mode of the CH_3 product for the $Cl+CH_4(\nu_{3b}=1) \rightarrow HCl(\nu=0)+CH_3(\nu_2)$ reaction at a collision energy of 0.159 eV.

Our results (from both the three- and four-dimensional models)[12,13] show that the CH_3 is most likely to form with two quanta in the umbrella mode. In contrast, to the experimental results, it was concluded that the umbrella mode excitation of CH_3 is negligible. This difference may be due to the approximate potential energy surface that was used in the dynamics calculations. Therefore, in the present work, this issue is addressed. A highly accurate potential energy surface is calculated and used to reinvestigate the quantum scattering dynamics of the $Cl+CH_4 \rightleftharpoons HCl+CH_3$ reaction. Furthermore, the deuterated reaction $Cl+CD_4 \rightleftharpoons DCl+CD_3$ has also been studied and compared with the most recent experimental results.[18]

II. POTENTIAL ENERGY SURFACE

In this study a semiempirical dual-level approach, scaling all the correlation (SAC) energy method,[19–21] has been used to calculate structures and energies of the $Cl+CH_4$ reaction. In the SAC approach, the resulting energy can be written as

$$E_{\mathrm{MP2/SAC}}=E_{\mathrm{HF}}+\frac{E_{\mathrm{MP2}}-E_{\mathrm{HF}}}{F}, \tag{1}$$

where E_{HF} and E_{MP2} denote Hartree–Fock and single reference Møller-Plesset second-order perturbation (MP2) energies, respectively. F is a constant scale factor which should be chosen to best balance the calculations of correlation en-

a)Electronic mail: nyman@phc.chalmers.se

TABLE I. Calculated and experimental geometrical parameters at the stationary points (lengths in a_0 and angles in degrees). R_i and α_c are shown in Fig. 1. TS denotes transition state.

Species	Parameters	MP2 (Refs. 9 and 10) [6-31$G(d)$]	MP2(FU) (Ref. 3) (TZ+2P)	MP2/SAC (Ref. 2) [MC-311(2d,d,p)]	This work	Expt. (Refs. 36 and 37)
HCl($C_{\infty V}$)	R_{HCl}	2.419	2.411	2.4115	2.4115	2.4086
CH_3(D_{3h})	R_{CH}	2.037	2.026	2.0403	2.0415	2.0390
CH_4(T_d)	R_{CH}	2.060	2.046	2.0607	2.0617	2.0617
$ClHCH_3$	R_1	2.704	2.744	2.7050	2.7068	
(C_{3V}, TS)	R_2	2.717	2.598	2.6231	2.6212	
	R_3	2.048	2.037	2.0519	2.0519	
	α_c	101.2	101.2	101.18	101.18	
$ClH\cdots CH_3$	R_1	2.432			2.434	
(C_{3V}, complex)	R_2	4.416			4.290	
	R_3	2.041			2.050	
	α_c	94.3			93.6	

ergies between/among the forming and breaking bonds by adjusting the basis sets. Gordon and Truhlar[19–21] have developed general scale factors for various types of bonds with several common basis sets. Also, for the $Cl+CH_4 \rightarrow HCl+CH_3$ reaction there is an optimized MC-311(2d,d,p) basis set, which was obtained by Truong *et al.*[2] Except for a small difference described below, the same basis set is employed here.

The MC-311(2d,d,p) basis set consists of a triple split 6-311G[22] basis set with polarization functions having exponential parameters $\alpha_p=0.75$ for the hydrogens and $\alpha_d=0.626$ for the carbon atom. The McLean–Chandler basis[23] with two polarization functions having exponential parameters $\alpha_d=1.04$ and 0.34 are used for the chlorine atom. At the MP2 level the correlation energy is calculated for both core and valence-shell electrons. The scale factor obtained is $F=0.8436$ which is an average of the values 0.8497, determined from the H–Cl bond dissociation energy, and 0.8375, determined from the H–C bond dissociation energy of CH_4.[2] This value is in good agreement with the value $F=0.835$ obtained by Truong *et al.*[2] in their MP2/SAC calculations. The minor difference comes from the use of different Cartesian functions for the polarization d functions. All calculations are carried out using a GAUSSIAN 94 code.[24]

Calculated geometries and normal mode frequencies for the stationary points are given in Tables I and II, which also include experimental and previous theoretical results. The present results are in excellent agreement with the MP2/SAC results obtained by Truong and Truhlar and co-workers.[2,4,6] This shows that the influence of using a slightly different scale factor F is very small. Both sets of calculations are in good agreement with the available experimental measurements as well as with other high level *ab initio* calculations.[3,9,10] From Table II it can, however, be seen that the H–C bond length R_2, see Fig. 1 for coordinate illustra-

TABLE II. Calculated and experimental harmonic normal mode vibrational frequencies (in cm^{-1}) for the molecules HCl, CH_3, and CH_4 and the transition state $ClHCH_3$(TS). The frequencies for the fully deuterated variants are given in parentheses.

Species	Mode	MP2(FU) (Ref. 3) (TZ+2P)	MP2/SAC (Refs. 2 and 6) (MC-311(2d,d,p))	This work[a]	Expt. (Refs. 36 and 37).
HCl	σ	3063	3030	**3030(2172)**	2991
CH_3	a_1'	3178	3165	3166(2240)	3002
	a_2''	460	436	**437(338)**	580
	e'	3369	3361	3361(2505)	3184
	e'	1441	1441	1435(1055)	1383
CH_4	a_1	3076	3065	3067(2170)	2917
	e	1591	1565	1563(1106)	1534
	t_1	3212	3210	**3212(2378)**	3019
	t_2	1369	1346	**1346(1017)**	1306
$ClHCH_3$	$\nu_1(a')$	3132	3118(2214)	3125(2219)	
(TS)	$\nu_2(a')$	1213	1227(956[b])	**1229(957)**	
	$\nu_3(a')$	511	572(484)	**573(485)**	
	$\nu_4(e)$	3305	3295(2451)	3302(2456)	
	$\nu_5(e)$	1448	1441(1056)	1436(1052)	
	$\nu_6(e)$	958	874(631)	926(667)	
	$\nu_7(e)$	378	324(232)	387(276)	
	$\nu_{\neq}(a')$	1262i	950i(746i)	**915i(722i)**	

[a]A bold face frequency indicates that a mode/the mode of that symmetry group is dynamically treated in the quantum scattering calculations.

[b]We have interchanged the frequencies 956 and 1056 compared to the values given in Table VII of Ref. 6.

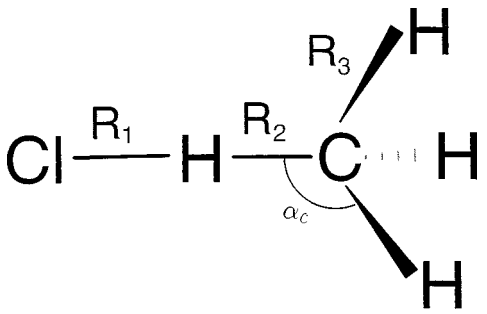

FIG. 1. Illustration of the coordinates used to describe the reaction $Cl+CH_4 \rightleftharpoons HCl+CH_3$ in C_{3V} symmetry.

tion, and the imaginary frequency at the saddle point are sensitive to the method used. Moreover, we also predict a Van der Waals complex $ClH\cdots CH_3$ (C_{3V} symmetry), which has a binding energy of 2.58 kcal/mol with $R_2=4.290\ a_0$. This complex was first discovered by Chen *et al.*[9] using G1 theory. They obtained a binding energy of 0.627 kcal/mol with a bond length $R_2=4.416a_0$ as shown in Table I. Then, Duncan and Truong[4] found that this complex lies 2.32 kcal/mol below the dissociation channel $HCl+CH_3$ at both the BH&HLYP and the PMP4/BH&HLYP levels, with R_2 being $4.248a_0$. In spite of the discrepancy in the binding energy, all calculations gave a loose structure.

In order to study the dynamics of the $Cl+CH_4$ reaction, we need to construct a potential energy surface. For a large system, it is a formidable task to build up a full dimensional surface using the *ab initio* method described above. Here, the calculations are restricted to C_{3V} symmetry. A motive for this is that the minimum energy path has C_{3V} symmetry. Further, we will use the surface to perform quantum scattering calculations[13] using the rotating line umbrella (RLU) model, which only accesses C_{3V} geometries. Additionally, as shown in Table I, the C–H bond length (R_3) changes only slightly between reactants and products. Throughout the calculations, the R_3 bond length is therefore for simplicity held fixed at $2.0519a_0$, i.e., the value at the transition state. More than 2000 energy points have been calculated. They cover the geometries defined by $R_1\in[1.80,4.63]a_0$, $R_2\in[0.85,4.25]a_0$, and $z\in[-1.97,1.97]a_0$, where z is the umbrella coordinate, i.e., the component of R_3 along the Cl–H–C axis.

The *ab initio* points have been fitted to an analytic many-body expansion expression,[25]

$$V(R_1,R_2,z)=V^{(1)}+V^{(2)}_{\mathrm{HCl}}(R_1)+V^{(2)}_{um}(z)+V^{(3)}_{\mathrm{CH_4}}(R_2,z)+V^{(3)}_{LR}(R_1,R_2)+V^{(4)}_{\mathrm{ClCH_4}}(R_1,R_2,z), \quad (2)$$

where $V^{(n)}$ is the n-body term. Here, the one-body term $V^{(1)}$ is a constant as the reaction does not involve any electronically excited species.

The two-body terms are written as

$$V^{(2)}_{um}(z)=(b_1+b_2z^2)z^2\exp(b_3z^2), \quad (3)$$

$$V^{(2)}_{\mathrm{HCl}}(R)=V_{\mathrm{GM}}(R;D_e,R_e,\beta,\lambda_1,\lambda_2) \quad (4)$$

with the five-parameter generalized Morse (GM) function,

$$V_{\mathrm{GM}}(R)=D_e[\exp(-2\alpha\Delta\rho)-2\exp(-\alpha\Delta\rho)] \quad (5)$$

and

$$\alpha=\beta(1+\lambda_1\Delta\rho+\lambda_2\Delta\rho^2),$$

$$\Delta\rho=R-R_e.$$

In Eq. (2), there are two three-body terms, one representing Hartree–Fock energy, $V^{(3)}_{\mathrm{CH_4}}(R_2,z)$, and the other representing correlation energy, $V^{(3)}_{LR}(R_1,R_2)$.[26] The Hartree–Fock energy term is also described by the GM function;

$$V^{(3)}_{\mathrm{CH_4}}(R_2,z)=V_{\mathrm{GM}}(R_2;D_e(z),R_e(z),\beta(z),\lambda_1(z),\lambda_2(z)), \quad (6)$$

where the five parameters $(D_e(z),R_e(z),\beta(z),\lambda_1(z),\lambda_2(z))$ explicitly depend on the umbrella coordinate z. They are represented by a Padé approximation, i.e.,

$$f(z)=\frac{a_1+a_2z+a_3z^2+a_4z^3}{1+a_5z+a_6z^2}. \quad (7)$$

The correlation energy term is used to approximately describe the long-range interaction potential. It is expressed as

$$V^{(3)}_{LR}(R_1,R_2)=-\left(\frac{R_1}{R_1^m}\right)^4\exp\left(-4\left(\frac{R_1}{R_1^m}-1\right)\right)\times\sum_{n=5}^{6}\frac{C_n\chi_n(R_1+R_2;R_1^m)}{(R_1+R_2)^n} \quad (8)$$

with the damping function

$$\chi_n(R;R^m)=\begin{cases}\{1-\exp[-A_n(R-R^m)-B_n(R-R^m)^2]\}^n & \text{if } R\geq R^m\\ 0 \quad \text{otherwise.}\end{cases} \quad (9)$$

The last term in Eq. (2) is a four-body term, which is written as a product of a fourth order polynomial $P(R_1,R_2,z)$ and a range function $T(R_1,R_2,z)$,

$$V^{(4)}_{\mathrm{ClCH_4}}(R_1,R_2,z)=P(R_1,R_2,z)T(R_1,R_2,z) \quad (10)$$

with

$$T=\exp(\gamma Q_3^2)\times\prod_{i=1}^{2}\left\{1-\tanh\left(\frac{1}{2}[\alpha_i(R_i-R_i^e)+\beta_i(R_i-R_i^e)^2]\right)\right\}, \quad (11)$$

$$P=\sum_{j,k,l}^{j+k+l\leq 4}c_{jkl}Q_1^jQ_2^kQ_3^l \quad (12)$$

and the coordinates Q_i

$$Q_1=R_1+R_2-R_1^e-R_2^e,$$

$$Q_2=R_1-R_2+R_2^e-R_1^e,$$

$$Q_3=z-z^e,$$

where (R_1^e,R_2^e,z^e) is a set of reference coordinates.

TABLE III. Parameters defined in Eqs. (2)–(12). The energy unit is eV, while lengths are in a_0.

One body	$V^{(1)}=4.318\,94$					
Two body						
$V^{(2)}_{um}$	$b_1=0.3808$		$b_2=0.465\,94$		$b_3=0.107\,72$	
$V^{(2)}_{\mathrm{HCl}}$	$D_e=4.084\,72$		$R_e=2.41\,15$		$\beta=1.042\,65$	
	$\lambda_1=0.055\,92$		$\lambda_2=0.101\,15$			
Three body						
$V^{(3)}_{LR}$	$C_5=1490.0$		$A_5=0.031\,05$		$B_5=0.096\,76$	
	$C_6=126\,75.0$		$A_6=0.041\,28$		$B_6=0.096\,75$	
	$R^m_1=2.4115$					
$V^{(3)}_{\mathrm{CH_4}}$	a_1	a_2	a_3	a_4	a_5	a_6
$D_e(z)$	3.460 21	1.190 70	1.668 78	1.047 41	−0.289 01	0.782 83
$R_e(z)$	2.157 83	1.827 86	0.354 31	0.0	0.907 85	0.195 15
$\beta(z)$	1.052 28	0.463 79	0.160 40	0.0	0.683 04	0.122 29
$\lambda_1(z)$	0.147 17	−0.0341	−0.012 51	0.0	1.110 86	0.348 14
$\lambda_2(z)$	0.181 94	0.189 26	0.100 79	0.0	0.905 32	0.211 09
Four body						
$c_{000}=2.343\,93$	$c_{001}=0.926\,39$		$c_{002}=-0.607\,26$		$c_{003}=-0.338\,68$	
$c_{004}=0.115\,35$	$c_{100}=-0.477\,56$		$c_{101}=0.401\,32$		$c_{102}=0.162\,60$	
$c_{103}=-0.074\,92$	$c_{200}=0.124\,54$		$c_{201}=-0.02024$		$c_{202}=0.085\,94$	
$c_{300}=-0.070\,22$	$c_{301}=0.008\,04$		$c_{010}=0.04229$		$c_{011}=-0.439\,61$	
$c_{012}=0.056\,80$	$c_{020}=-0.210\,01$		$c_{021}=-0.091\,59$		$c_{022}=0.025\,43$	
$c_{110}=0.399\,11$	$c_{120}=-0.081\,84$		$c_{210}=0.028\,92$		$c_{220}=0.012\,90$	
$c_{111}=0.063\,91$	$c_{112}=-0.117\,40$		$c_{121}=-0.179\,61$		$c_{211}=0.088\,78$	
$c_{030}=-0.057\,07$	$c_{031}=-0.056\,44$		$c_{013}=0.092\,76$		$c_{400}=0.052\,99$	
$c_{040}=0.037\,61$	$\alpha_1=0.777\,93$		$\alpha_2=1.628\,82$		$\beta_1=0.668\,51$	
$\beta_2=0.213\,79$	$\gamma=0.239\,45$		$R^e_1=2.859\,73$		$R^e_2=2.779\,67$	
$z^e=0.112\,45$	$c_{130}=c_{310}=0.000\,00$					

The parameters in Eqs. (2)–(12) are fitted to 1136 *ab initio* energy points, which have an energy less than 3.0 eV with respect to the $Cl+CH_4$ dissociation limit. Points having higher energy are hardly accessed in the dynamics calculations and are therefore discarded before performing the nonlinear least-square fitting. The values obtained for the parameters are listed in Table III. The fitted potential gives an overall root-mean-square error of 0.8 kcal/mol and smaller deviations along the reaction path. No unphysical feature has been found on the surface. Figure 2 shows some comparisons between fitted curves and *ab initio* data for the two-body terms and the $V^{(3)}_{\mathrm{CH_4}}$ term. It can be seen that the agreement is good.

Figure 3 displays a contour plot for the analytic $Cl+CH_4 \rightleftharpoons HCl+CH_3$ potential energy surface. The transition state is at $R_1=2.730a_0$, $R_2=2.588a_0$, and $\alpha_c=101°$. The classical forward barrier height is 6.95 kcal/mol and there is an endoergicity of 5.40 kcal/mol, in good agreement with the MP2/SAC results, 6.87 kcal/mol and 5.98 kcal/mol, respectively. In addition, a loose complex is obtained at $R_2=4.200a_0$ with a binding energy of 2.24 kcal/mol. Again, these results are consistent with the *ab initio* results reported above.

Before the quantum dynamics calculations are done, a zero point energy correction is made, which relates to the degrees of freedom not explicitly treated in the dynamics study. Otherwise a negative adiabatical vibrational ground-state barrier height ($\Delta V^G_{a,r}$) would be obtained for the reverse reaction $HCl+CH_3 \rightarrow Cl+CH_4$. The correction was done by adding an extra term into the potential given in Eq. (2) to obtain an effective surface,

$$V_{\mathrm{eff}}(R_1,R_2,z)=V(R_1,R_2,z)+\Delta V_{\mathrm{corr}} \tag{13}$$

with

$$\Delta V_{\mathrm{corr}}=\frac{1}{2}V_c\{1-\tanh[\,\eta(R_2-R_\eta)]\}, \tag{14}$$

where the parameters are $\eta=1.32a_0^{-1}$, $R_\eta=4.16a_0$, and $V_c=0.135\,15$ eV for $Cl+CH_4$. For its isotopic variant $Cl+CD_4$, V_c' is set to $V_c/\sqrt{2}$. For these effective potentials, some important energetic properties are given in Table IV with the experimental and the previous theoretical results of Roberto-Neto *et al.*[6] for comparison. It is seen that the present results are in good agreement with the experimental ones as well as with the theoretical values. The structures of the transition states determined from the effective potential energy surfaces are given in Table V.

III. QUANTUM DYNAMICS AND FORMULATION

In the quantum scattering calculations a three dimensional rotating line umbrella (RLU) model is used. Since this model has been well described elsewhere,[12,27] except for a small improvement of the kinetic energy operator in the z coordinate, we only present a brief review here. The dynamics study is performed in the hypercylindrical coordinates (ρ,φ,z). The Hamiltonian of the system is expressed as

$$\hat{H}(\rho,\varphi,z)=-\frac{\hbar^2}{2\mu}\left[\frac{1}{\rho^3}\frac{\partial}{\partial\rho}\rho^3\frac{\partial}{\partial\rho}+\frac{1}{\rho^2}\frac{\partial^2}{\partial\varphi^2}\right]-\frac{\hbar^2}{2}\frac{\partial}{\partial z}G(z)\frac{\partial}{\partial z}+\frac{\hat{J}^2}{2I(z)}+V(\rho,\varphi,z) \tag{15}$$

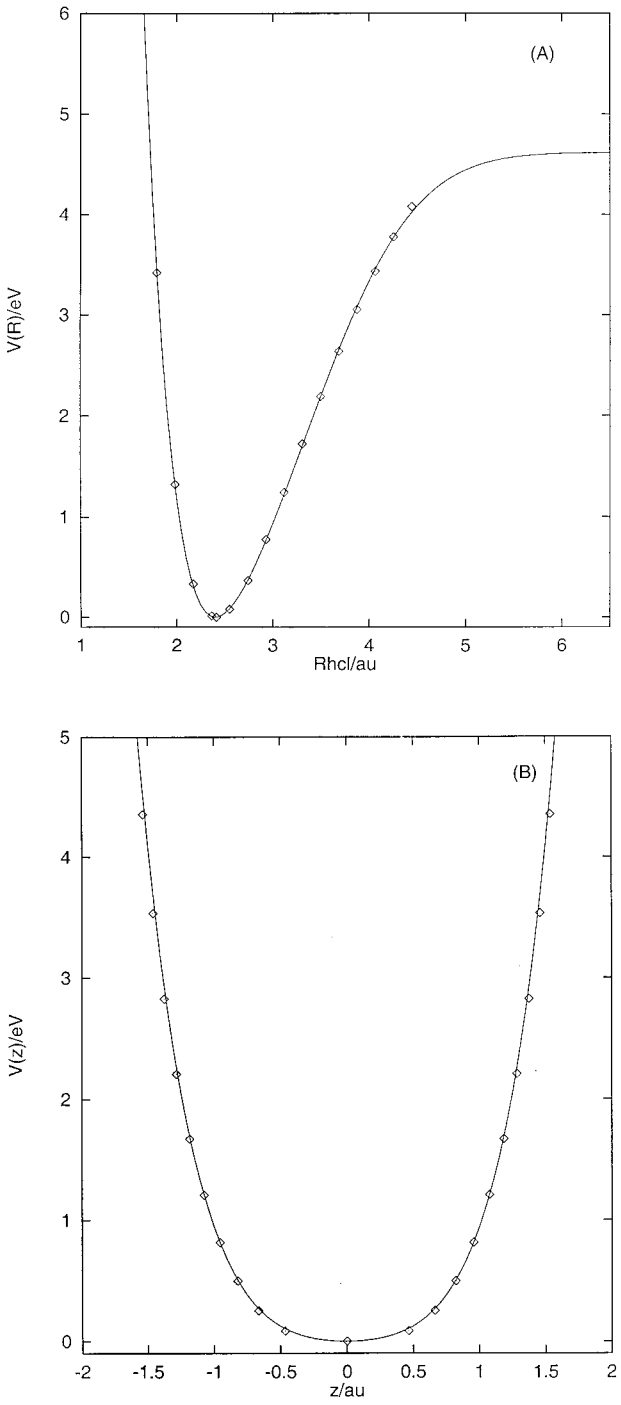

FIG. 2. Comparison of fitted potential energy surface (solid lines) with the *ab initio* data (open squares). (A) two-body HCl potential $V^{(2)}_{\mathrm{HCl}}(R)$; (B) two-body CH_3 potential $V^{(2)}_{um}(z)$, and (C) three-body CH_4 potential $V^{(3)}_{\mathrm{CH_4}}(R,z)$ at a few z values.

with the volume element

$$d\tau=\rho^3\,d\rho\,d\varphi\,dz\sin\theta\,d\theta\,d\phi,$$

where

$$I(z)=\mu\rho^2+\mu_z z^2,$$

$$\mu=\left[\frac{m_{\mathrm{Cl}}m_{\mathrm{H}}(m_{\mathrm{C}}+3m_{\mathrm{H}})}{m_T}\right]^{1/2},$$

$$\mu_z=\frac{3m_{\mathrm{C}}m_{\mathrm{H}}}{m_{\mathrm{C}}+3m_{\mathrm{H}}},$$

$$m_T=m_{\mathrm{Cl}}+m_{\mathrm{H}}+m_{\mathrm{C}}+3m_{\mathrm{H}},$$

$$G(z)=\frac{R_3^2-z^2}{\mu_z(R_3^2+3m_{\mathrm{H}}z^2/m_{\mathrm{C}})},$$

and the total angular momentum operator is

$$\hat{J}^2=-\hbar^2\left[\frac{1}{\sin\theta\partial\theta}\frac{\partial}{}\sin\theta\frac{\partial}{\partial\theta}+\frac{1}{\sin^2\theta}\frac{\partial^2}{\partial\phi^2}\right]. \tag{16}$$

Here m_{Cl}, m_{C}, and m_{H} are the masses of the Cl, C, and H atoms, respectively. (θ,ϕ) are the spherical angles describing the spatial orientation of the linear Cl–H–CH_3 molecule. In Eq. (15), $V(\rho,\varphi,z)$ is the effective potential energy sur-

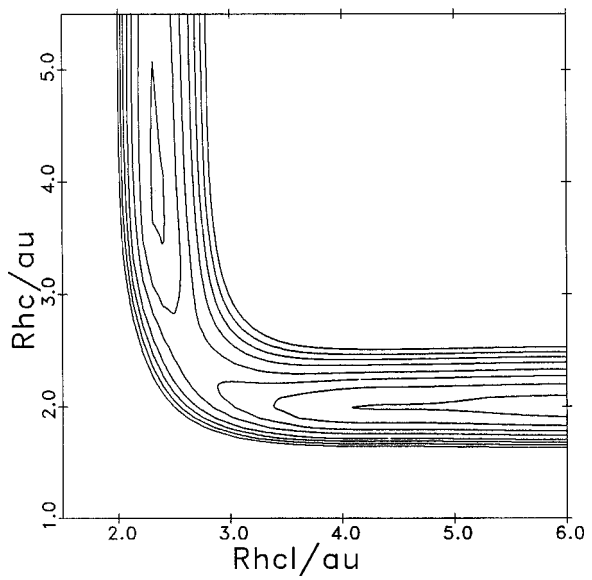

FIG. 3. Contour plot of the potential energy surface for the reaction $Cl+CH_4 \rightleftharpoons HCl+CH_3$, where the umbrella coordinate is optimized. The contours start at 1.0 kcal/mol with an interval of 2.5 kcal/mol. Energies are relative to the $Cl+CH_4$ limit.

face, which has been given in the preceding section. The other symbols have their usual meanings. The above Hamiltonian is hermitian and exact for the RLU model, where only geometries with C_{3v} symmetry are considered and the R_3 bond length is fixed.

A partial wave expansion method using spherical harmonics, $Y_J^0(\theta,\phi)$, has been employed to solve the time independent Schrödinger equation of the system. For a total angular momentum J and an initial quantum state m, the total wave function is expanded as

TABLE IV. Energetic properties (in kcal/mol) for the forward and reverse reactions from the three dimensional effective analytic potential energy surfaces. Harmonic frequencies from the effective surfaces are used when zero-point energies are required. The tabulated data for the effective surfaces are: endoergicity (ΔE), endothermicity at 0 K (ΔH_0), endothermicity at 298 K (ΔH_{298}), forward classical barrier height (ΔE_f^b), vibrationally adiabatic ground state barrier height ($\Delta V_{a,f}^G$) and classical barrier height (ΔE_r^b) and vibrationally adiabatic ground state barrier height ($\Delta V_{a,r}^G$) for the reverse reaction.

	$Cl+CH_4$			$Cl+CD_4$	
	This work	MP2/SAC (Ref. 6)[a]	Expt. (Refs. 1, 38, and 39)	This work	MP2/SAC (Ref. 6)[b]
ΔE	2.29	3.13		3.20	4.17
ΔH_0	1.19	1.20		2.29	2.18
ΔH_{298}	1.79	1.80	1.72		
ΔE_f^b	6.91	7.50		6.92	7.36
$\Delta V_{a,f}^G$	3.36	3.56	3.5	4.43	4.71
ΔE_r^b	4.62	4.37		3.72	3.19
$\Delta V_{a,r}^G$	2.17	1.96	1.5	2.14	1.81

[a]The basis set used was MC-311$(2d,d,p)$. We have used their frequencies to add zero-point energies to get the corresponding effective energy values that are directly comparable to our effective surface.

[b]As under *a* but using our calculated frequencies given in Table II for DCl, CD_3, and CD_4.

TABLE V. Transition states for the three dimensional effective potential energy surfaces (distances in a_0 and angles in degrees).

	R_1	R_2	R_3(fixed)	α_c
$ClHCH_3$	2.7338	2.5824	2.0519	101.2
$ClDCD_3$	2.7328	2.5838	2.0519	101.1

$$|\Psi_m(E)\rangle = \sum_J A_m^J |\psi_m^J\rangle Y_J^0(\theta,\phi), \tag{17}$$

where A_m^J are expansion coefficients satisfying asymptotic boundary conditions. Further, by dividing the hyperradius ρ into sectors i, the functions $|\psi_m^J\rangle$ are expanded in the coupled channel form

$$|\psi_m^J(\rho,\varphi,z)\rangle = \rho^{-3/2}\sum_{i=1}^{L}\sum_{n=1}^{N} h_{nm}(\rho;i,J)|H_n(\varphi,z;i,J)\rangle. \tag{18}$$

Then, the coupled channel equations can be written as

$$\frac{d^2}{d\rho^2}h_{nm}(\rho;i,J) + \sum_{n'=0}^{N}(\mathbf{D}_{\mathrm{H}})_{nn'}h_{n'm}(\rho;i,J) = 0, \tag{19}$$

where the coupling matrix has elements

$$(\mathbf{D}_{\mathrm{H}})_{nn'} = -\frac{2\mu}{\hbar^2}\left\{\left(\epsilon_n^H - E + \frac{3\hbar^2}{8\mu\rho^2}\right)\delta_{nn'} + \langle H_n|V - V_{\mathrm{H}}(\varphi,z;i,J) + \frac{J(J+1)\hbar^2}{2I(z)}|H_{n'}\rangle\right\}, \tag{20}$$

In Eq. (18), $|H_n(\varphi,z;i,J)\rangle$ are the eigenstates of a reference Hamiltonian, e.g., the Hamiltonian in Eq. (15) for fixed ρ. These states are obtained by solving,

$$\left[-\frac{\hbar^2}{2\mu\rho_i^2}\frac{\partial^2}{\partial\varphi^2} - \frac{\hbar^2}{2}\frac{\partial}{\partial z}G(z)\frac{\partial}{\partial z} + V_{\mathrm{H}}(\varphi,z;i,J) - \epsilon_n^H(i,J)\right] \times |H_n(\varphi,z;i,J)\rangle = 0, \tag{21}$$

where $V_{\mathrm{H}}(\varphi,z;i,J)$ is a reference potential at the sector i. The eigenpairs are found using a guided spectral transform Krylov subspace iteration approach[13,27] in a direct product discrete variable representation (DVR) basis set. Here, we have used sine-DVRs in φ and a Fourier basis in z.

The coupled channel equations in Eq. (19) were solved using the improved log-derivative algorithm of Manolopoulos.[28,29] The scattering matrix S has been extracted from the log-derivative matrix $\mathbf{Y}(\rho_i)$ at a large value of ρ_i using the hyperspherical projection method.[12] The S-matrix is given by

$$S^J(E) = -\mathbf{k}^{1/2}\mathbf{W}^{-1}\mathbf{W}^*\mathbf{k}^{-1/2} \tag{22}$$

with

$$\mathbf{W} = [\mathbf{Y}(\rho_i)X^{(1)} - X^{(3)}] + i[\mathbf{Y}(\rho_i)X^{(2)} - X^{(4)}] \tag{23}$$

and $\mathbf{k}$ is a diagonal matrix with the elements $(\mathbf{k})_{n'n} = k_n\delta_{n'n}$, where $k_n = \sqrt{2\mu(E-\epsilon_n^H)}$.

The matrices $\mathbf{X}^{(i)}$ in Eq. (22) are given (for a large value of ρ) by[12,13]

$$X^{(1)}_{kn}=\rho^{1/2}\langle H_k(\varphi,z;i,J)|R^{-1/2}\hat{y}_I(k_nR;J)|H_n(\varphi,z;i,J)\rangle,$$

$$X^{(2)}_{kn}=\rho^{1/2}\langle H_k(\varphi,z;i,J)|R^{-1/2}\hat{n}_I(k_nR;J)|H_n(\varphi,z;i,J)\rangle,$$

$$\begin{aligned}X^{(3)}_{kn}=&\rho^{-1/2}\langle H_k(\varphi,z;i,J)|R^{-1/2}\Bigg\{k_nR\hat{y}'_I(k_nR;J)\\&+\frac{1}{2}\left[1+\left(\frac{r}{\rho}\right)^2\right]\hat{y}_I(k_nR;J)\Bigg\}|H_n(\varphi,z;i,J)\rangle\\&+\rho^{-1/2}\langle H_k(\varphi,z;i,J)|\pm\frac{r\sqrt{R}}{\rho^2}\hat{y}_I(k_nR;J)\\&\times|H'_n(\varphi,z;i,J)\rangle,\end{aligned}$$

$$\begin{aligned}X^{(4)}_{kn}=&\rho^{-1/2}\langle H_k(\varphi,z;i,J)|R^{-1/2}\Bigg\{k_nR\hat{n}'_I(k_nR;J)\\&+\frac{1}{2}\left[1+\left(\frac{r}{\rho}\right)^2\right]\hat{n}_I(k_nR;J)\Bigg\}|H_n(\varphi,z;i,J)\rangle\\&+\rho^{-1/2}\langle H_k(\varphi,z;i,J)|\pm\frac{r\sqrt{R}}{\rho^2}\hat{n}_I(k_nR;J)\\&\times|H'_n(\varphi,z;i,J)\rangle,\end{aligned}\tag{24}$$

and

$$H'_n(\varphi,z;i,J)=\frac{\partial H_n(\varphi,z;i,J)}{\partial\varphi},\tag{25}$$

where the ''+'' and ''−'' refer to the reactant ($Cl+CH_4$) and product ($HCl+CH_3$) channels, respectively. $\hat{y}_I(x)$, $\hat{n}_I(x)$, $\hat{y}'_I(x)$, and $\hat{n}'_I(x)$ are the real Riccati–Bessel functions and their derivatives, respectively.

From the S-matrix, the state-to-state reaction probability for the reaction $Cl+CH_4(\nu_{3b},\nu_4)\rightarrow HCl(\nu)+CH_3(\nu_2)$ is obtained as

$$P^J_{\nu_{3b}\nu_4\rightarrow\nu\nu_2}=|S^J_{\nu_{3b}\nu_4\rightarrow\nu\nu_2}|^2,\tag{26}$$

where the vibrational quantum numbers ν, ν_{3b}, ν_2, and ν_4 refer to the H–Cl stretch, the reactive H–C stretch and the umbrella modes in CH_3 and CH_4, respectively. The cumulative reaction probability (CRP), $N(E,J)$, can be calculated by summing the state-to-state reaction probabilities over all final and initial states, i.e.,

$$N(E,J)=\sum_{\nu_{3b}\nu_4}\sum_{\nu\nu_2}P^J_{\nu_{3b}\nu_4\rightarrow\nu\nu_2}.\tag{27}$$

Differential cross sections $d\sigma_{\nu_{3b}\nu_4\rightarrow\nu\nu_2}(\theta_R)/d\Omega$ and integral cross sections $\sigma_{\nu_{3b}\nu_4\rightarrow\nu\nu_2}$ for going from the initial state (ν_{3b},ν_4) to the final state (ν,ν_2) are obtained from[30]

$$\begin{aligned}\frac{d\sigma_{\nu_{3b}\nu_4\rightarrow\nu\nu_2}}{d\Omega}(\theta_R)=&\frac{1}{4k^2_{\nu_{3b}\nu_4}}\Bigg|\sum_J(2J+1)\\&\times S^J_{\nu_{3b}\nu_4\rightarrow\nu\nu_2}P_J(\cos(\pi-\theta_R))\Bigg|^2,\end{aligned}\tag{28}$$

$$\sigma_{\nu_{3b}\nu_4\rightarrow\nu\nu_2}=\frac{\pi}{k^2_{\nu_{3b}\nu_4}}\sum_J(2J+1)P^J_{\nu_{3b}\nu_4\rightarrow\nu\nu_2},\tag{29}$$

where $k_{\nu_{3b}\nu_4}$ is the initial translational wave number corresponding to the vibrational state (ν_{3b},ν_4) of CH_4 and P_J are Legendre polynomials. In Eq. (28) we have used $(\pi-\theta_R)$ in one place rather than θ_R in order to keep the definition of forward scattering consistent with the experimental convention, i.e., $\theta_R=0$ corresponds to forward scattering and $\theta_R=\pi$ to backward scattering.

The thermal rate constant is calculated from[31,32]

$$k(T)=\frac{Q(T)Q^{\ddagger}_{\rm rot}(T)}{2\pi\hbar Q_r(T)}\int_{-\infty}^{+\infty}dE\,\exp\{-E/kT\}N(E,J=0),\tag{30}$$

where $Q(T)$ is the partition function at the transition state for all vibrational modes not explicitly treated in the RLU scattering calculations, $Q^{\ddagger}_{\rm rot}(T)$ is the rigid rotor symmetric top approximation for the rotational partition function of the CH_4Cl complex, $Q_r(T)$ is the reactant partition function per unit volume and $N(E,J=0)$ is the CRP evaluated for $J=0$. This treatment for $k(T)$ is equivalent to using the J-shifting approximation[33] and assuming that the degrees of freedom not treated explicitly are separable.

Vibrationally state-selected rate constants $k_{\nu_{3b}\nu_4}(T)$ for the reaction $Cl+CH_4(\nu_{3b},\nu_4)\rightarrow HCl+CH_3$ are calculated from

$$\begin{aligned}k_{\nu_{3b}\nu_4}(T)=&\frac{Q(T)Q^{\ddagger}_{\rm rot}(T)}{2\pi\hbar Q'_r(T)}\int_{-\infty}^{+\infty}dE\\&\times\exp\{-E/kT\}N_{\nu_{3b}\nu_4}(E-\epsilon^H_{\nu_{3b}\nu_4},J=0),\end{aligned}\tag{31}$$

where $Q'_r(T)$ is the reactant partition function per unit volume but excluding the contribution from the two vibrational modes (ν_{3b},ν_4) of CH_4. $N_{\nu_{3b}\nu_4}(E-\epsilon^H_{\nu_{3b}\nu_4},J=0)$ is the reaction probabilities out of the initial state (ν_{3b},ν_4) summed over all product states and $\epsilon^H_{\nu_{3b}\nu_4}$ is the vibrational energy of that state. For the reverse reaction, there is a similar expression.

The ground state tunneling coefficient, η^G, and transmission coefficient, κ^G, are defined as[34]

$$\eta^G=\frac{\displaystyle\int_{-\infty}^{+\infty}dE\,\exp\{-E/kT\}N_0(E,J=0)}{\displaystyle\int_{E^*}^{+\infty}dE\,\exp\{-E/kT\}N_0(E,J=0)},\tag{32}$$

$$\kappa^G=\frac{1}{kT}\exp\left\{\frac{E^*}{kT}\right\}\int_{-\infty}^{+\infty}dE\,\exp\{-E/kT\}N_0(E,J=0),\tag{33}$$

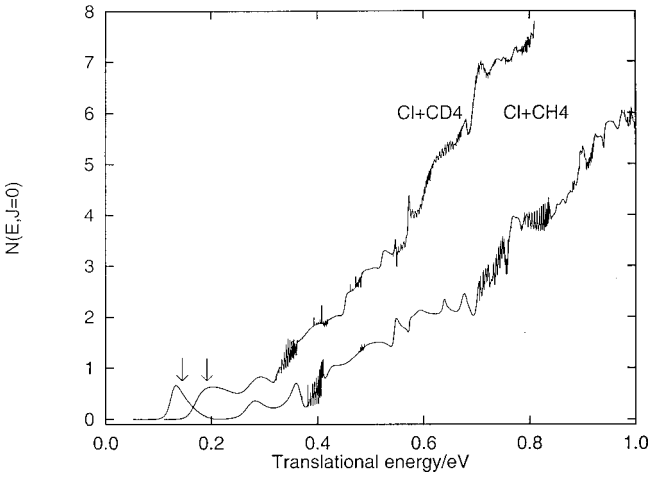

FIG. 4. Cumulative reaction probabilities for the $Cl+CH_4 \rightleftharpoons HCl+CH_3$ and $Cl+CD_4 \rightleftharpoons DCl+CD_3$ reactions for total angular momentum $J=0$. The arrows indicate the positions of the vibrationally adiabatic ground state threshold energy (E^*). Energies are measured from the potential bottom of the reactant channel.

where E^* is the vibrationally adiabatic ground state threshold energy determined from the effective potential energy surfaces and N_0 is the reaction probability out of the reaction ground state summed over all product states.

The reactant geometries used in evaluating the partition functions in Eqs. (30) and (31) can be found in Table I, while the transition state geometries are taken from Table V. The frequencies used are taken from Table II. The procedures employed are the same as in Ref. 12.

IV. RESULTS AND DISCUSSION

In the scattering calculations, the coupling matrix was expressed in a direct product DVR basis. For the $Cl+CH_4 \rightleftharpoons HCl+CH_3$ reaction, we have used 110 sine-DVRs for φ and 40 Fourier DVRs for z, spanning the range $[-1.65,1.65]a_0$. For $Cl+CD_4 \rightleftharpoons DCl+CD_3$, 120 sine-DVRs and 49 Fourier DVRs were employed, respectively.

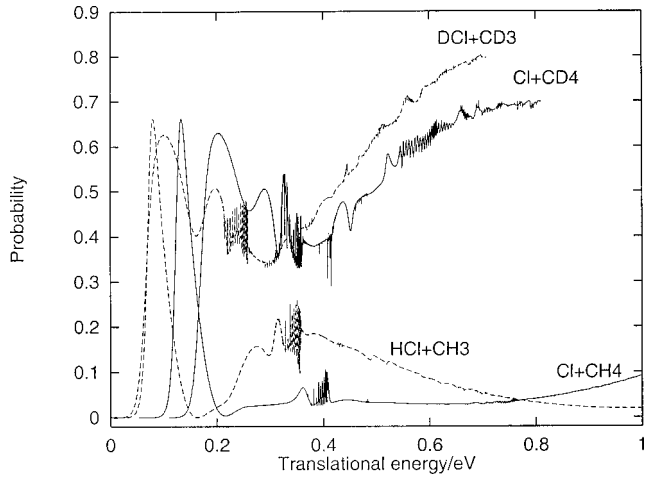

FIG. 5. Reaction probabilities out of the ground-state as a function of translational energy for the $Cl+CH_4 \rightleftharpoons HCl+CH_3$ and $Cl+CD_4 \rightarrow DCl+CD_3$ reactions for $J=0$, summed over all product modes in each case. Solid and dashed lines refer to the forward and reverse reactions, respectively.

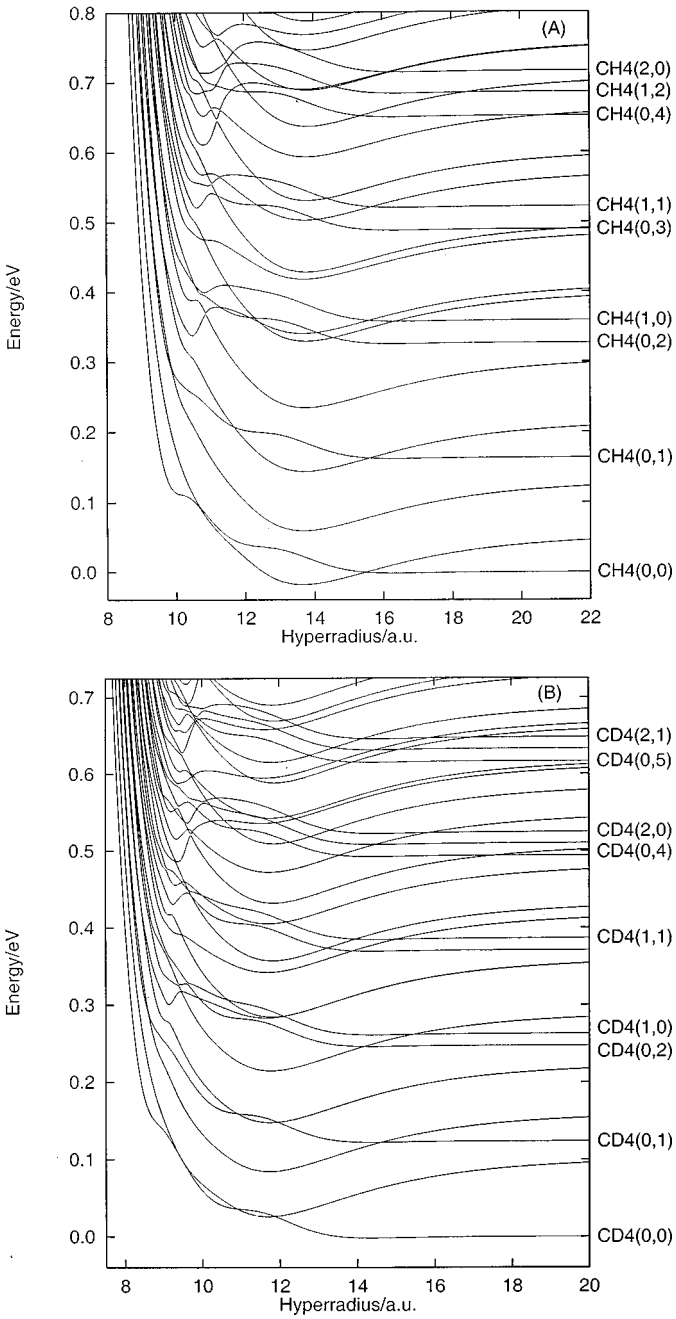

FIG. 6. Hyperspherical adiabatic energy levels as a function of the hyperradius for $J=0$. Some adiabats are labeled as $CH_4(\nu_{3b},\nu_4)$ or $CD_4(\nu_{3b},\nu_4)$ in the asymptotic limit. (A) for the $Cl+CH_4 \rightleftharpoons HCl+CH_3$ reaction, and (B) for the $Cl+CD_4 \rightleftharpoons DCl+CD_3$ reaction.

Then, a contracted basis set was constructed by truncating those DVRs where the potential energies are higher than a threshold energy $V_{th}=3.5$ eV relative to the potential bottom of $Cl+CH_4/CD_4$. The surface functions were computed by an exponential guided spectral transform (GST) Krylov subspace iteration algorithm. A detailed presentation of the algorithm has been given in Refs. 13 and 27.

The coupled channel equations were solved by the quasi-adiabatic log-derivative algorithm.[28,29] The propagation was performed from $\rho=6.5a_0$ to $\rho=28.5a_0$ using 567/607 sectors for CH_4/CD_4 with an adiabatic basis of 70 functions. The S matrix was calculated using the single-sector hyperspherical projection method summarized above.

TABLE VI. Calculated and experimental thermal rate constants ($k(T)$/cm^3 s^{-1} molecule^{-1}), ground state rate constants ($k_G(T)$) and ground-state tunneling (η^G) and transmission (κ^G) coefficients for the reaction $Cl+CH_4 \rightarrow HCl+CH_3$.

T/K	$k(T)$	$k_G(T)$	η^G	κ^G	Expt. (Ref. 39)	Expt. (Ref. 38)	Expt. (Ref. 8)	Expt. (Ref. 7)
200	7.90(−15)	7.90(−15)	8.74	2.69	1.1(−14)		1.1(−14)	
250	2.85(−14)	2.85(−14)	6.50	1.80	4.1(−14)		4.3(−14)	
300	6.81(−14)	6.81(−14)	5.39	1.36	1.0(−13)	9.4(−14)	1.0(−13)	1.04(−13)
350	1.29(−13)	1.29(−13)	4.73	1.09				1.8(−13)
400	2.11(−13)	2.10(−13)	4.29	0.92	3.5(−13)	3.4(−13)	3.1(−13)	3.0(−13)
500	4.36(−13)	4.31(−13)	3.76	0.70	8.8(−13)	7.5(−13)	8.2(−13)	6.5(−13)
600	7.33(−13)	7.16(−13)	3.43	0.57				1.7(−12)
800	1.53(−12)	1.42(−12)	3.04	0.42				

A. Reaction probability and adiabats

Figure 4 shows cumulative reaction probabilities as a function of translational energy. The probabilities show structure as observed in our previous work.[11–13] In particular, the existence of the van der Waals complex has caused clusters of narrow resonances. The cumulative reaction probability increases rapidly when the translational energy is higher than 0.35–0.40 eV. The translational energy enhancement of the reactivity is larger for $Cl+CD_4 \rightleftharpoons DCl+CD_3$ than for $Cl+CH_4 \rightleftharpoons HCl+CH_3$. Even so, relative to the number of accessible channels, the $Cl+CD_4$ cumulative reaction probabilities are significantly smaller. In addition, Fig. 4 clearly shows a pronounced tunneling effect for both the $Cl+CH_4 \rightleftharpoons HCl+CH_3$ and the $Cl+CD_4 \rightleftharpoons DCl+CD_3$ reactions. Thus, there are substantial quantum effects in these reactions.

Reaction probabilities out of the ground state, summed over all product states, are displayed in Fig. 5 for both the forward and the reverse reactions. The ground-state tunneling effects are clearly demonstrated. It can also be seen that there is a noticeable isotope effect. For the $Cl+CH_4 \rightleftharpoons HCl+CH_3$ reaction, except for the tunneling peak, the reaction probabilities are small. That is, at high energies, the ground-state process $Cl+CH_4(0,0) \rightleftharpoons HCl(0)+CH_3(0)$ is of little importance. On the other hand, for the $Cl+CD_4 \rightleftharpoons DCl+CD_3$ reaction, the ground-state reaction probabilities are large and approach 0.7 as the kinetic energy is increased.

The propensities of the reaction probabilities can be illustrated by the hyperspherical adiabats shown in Fig. 6. For instance, the wells on curves correlating to the $HCl/DCl+CH_3/CD_3$ channels in the asymptotic limit result in the resonances. Furthermore, there are many strong correlations between the reactant and the product channels in the region $\rho \in [10.0,12.0]a_0$ for the $Cl+CD_4 \rightleftharpoons DCl+CD_3$ reaction, which may explain the difference in reactivity compared to the $Cl+CH_4 \rightleftharpoons HCl+CH_3$ reaction.

B. Thermal rate constant, tunneling and isotope effect

Table VI contains the calculated thermal rate constants, ground-state rate constants and ground-state tunneling and transmission coefficients together with experimental results for the $Cl+CH_4 \rightleftharpoons HCl+CH_3$ reaction. The theoretical thermal rate constants are approximately 50% smaller than the measured values. In the temperature range 200–800 K, however, the overall agreement is good. The underestimation may be due to the reduced dimensionality approximation used in the dynamics model. Our recent studies using a model including nonlinear geometries, the four dimensional rotating bond umbrella (RBU) approximation, gave larger rate constant than the RLU model.[13,35] Of course, other factors, such as the use of the J-shifting approximation, could also introduce errors. It can be seen from Table VI that the reaction predominantly occurs out of the ground-state according to the calculations. Also, as discussed above, the tunneling (η^G) and recrossing (η^G/κ^G) effects are large.

For the reverse reaction $HCl+CH_3 \rightarrow Cl+CH_4$, the calculated results together with experimental measurements are given in Table VII. The experimental and calculated thermal rate constants are in fairly good agreement. Further, it can be seen that the ground-state rate constants are larger than the thermal ones. This has been explained previously by the fact that exciting the umbrella mode of the CH_3 radical impedes the reaction.[12,13]

Table VIII gives calculated thermal rate constants, ground-state rate constants and ground-state tunneling and transmission coefficients for the $Cl+CD_4 \rightleftharpoons DCl+CD_3$ reactions. As expected, it is found that the tunneling and recrossing effects are reduced for both the forward and reverse processes compared to the normal isotope reactions. Also, the rate constants for the deuterated reactions show stronger temperature dependence than the $Cl+CH_4 \rightleftharpoons HCl+CH_3$ reaction. Nevertheless, the overall trends of the rate constants are similar for these isotopic variants.

Calculated kinetic isotope effects are listed in Table IX.

TABLE VII. Calculated and experimental thermal rate constants ($k(T)$/cm^3 s^{-1} molecule^{-1}), ground state rate constants ($k_G(T)$) and ground-state tunneling (η^G) and transmission (κ^G) coefficients for the reaction $HCl+CH_3 \rightarrow Cl+CH_4$.

T/K	$k(T)$	$k_G(T)$	η^G	κ^G	Expt. (Ref. 38)	Expt. (Ref. 40)
200	2.21(−14)	2.31(−14)	10.05	2.92		
250	3.34(−14)	3.63(−14)	7.37	1.93		
300	4.26(−14)	4.84(−14)	6.04	1.44	4.8(−14)	6.6(−14)
350	4.98(−14)	5.93(−14)	5.25	1.15	6.7(−14)	1.10(−13)
400	5.54(−14)	6.92(−14)	4.73	0.96	8.6(−14)	1.6(−13)
500	6.42(−14)	8.72(−14)	4.05	0.73	1.2(−13)	2.8(−13)
600	7.15(−14)	1.05(−13)	3.63	0.59		
800	8.75(−14)	1.40(−13)	3.06	0.44		

TABLE VIII. Calculated thermal rate constants ($k(T)$/cm^3 s^{-1} molecule^{-1}), ground state rate constants ($k_G(T)$), and ground-state tunneling (η^G) and transmission (κ^G) coefficients for the forward and reverse reactions $Cl+CD_4 \rightleftharpoons DCl+CD_3$.

	$Cl+CD_4$				$DCl+CD_3$			
T/K	$k(T)$	$k_G(T)$	η^G	κ^G	$k(T)$	$k_G(T)$	η^G	κ^G
200	3.31(−16)	3.31(−16)	5.00	3.03	8.26(−15)	8.96(−15)	5.98	3.59
250	2.29(−15)	2.28(−15)	3.50	2.10	1.32(−14)	1.52(−14)	4.06	2.39
300	8.84(−15)	8.79(−15)	2.81	1.66	1.84(−14)	2.23(−14)	3.18	1.84
350	2.43(−14)	2.40(−14)	2.41	1.40	2.37(−14)	3.03(−14)	2.69	1.53
400	5.35(−14)	5.27(−14)	2.16	1.24	2.91(−14)	3.92(−14)	2.38	1.34
500	1.73(−13)	1.68(−13)	1.85	1.04	4.06(−14)	5.92(−14)	2.01	1.10
600	4.04(−13)	3.85(−13)	1.68	0.92	5.37(−14)	8.29(−14)	1.80	0.96
800	1.30(−12)	1.18(−12)	1.49	0.79	8.59(−14)	1.42(−13)	1.57	0.81

There are no experimental data for the reverse reaction, so we use the previous theoretical values of Chen *et al.*[10] to compare to. It is seen that the present calculations are in reasonably good agreement with the results by Chen *et al.*,[10] although we obtain smaller isotope effects. One reason for this may be that the MP2/SAC method gives a slightly smaller imaginary frequency at saddle point compared both to that calculated by MP2/MC-311$(2d,d,p)^2$ and from the semiempirical potential energy surfaces used by us.[11,13] As a result, the tunneling effects obtained here are smaller than in the previous work,[11,13] which could affect the isotope effects. Most recently, Roberto-Neto *et al.*[6] have also noticed that using the larger imaginary frequency at the transition state from MP2 level calculations instead of the MP2/SAC method frequency gives a better agreement for the kinetic isotope effect when comparing to experimental results.

The kinetic isotope effect for the forward reactions is larger and more temperature dependent than that of the reverse reactions. The calculated isotope effect for the forward reactions is, however, smaller than the experimental results, which again could be related to a too small value of the imaginary frequency at the transition state.

C. Differential cross section

We have found that the differential cross sections, calculated using the potential energy surface developed in this work, for the $Cl+CH_4(0,0)$ and $Cl+CH_4(1,0)$ reactions show the same behavior as reported before,[11–13] and they will not be shown here. It is, however, worthwhile to mention that substantial excitation of the umbrella mode of the CH_3 product for $Cl+CH_4(1,0) \rightarrow HCl(0)+CH_3(\nu_2)$ is still predicted. This is inconsistent with the experimental measurements, which suggest only a small excitation of the umbrella mode.[16] All other properties investigated for the $Cl+CH_4$ reaction are however qualitatively in good agreement with the experimental results. For a kinetic energy of 0.159 eV, some calculated cross sections are listed in Table X.

Recently, Kandel and Zare[18] measured the differential cross sections for the $Cl+CD_4(0,0) \rightarrow DCl(0)+CD_3$ reaction at a few collision energies. We have therefore calculated differential cross section at 0.15, 0.18, 0.22, and 0.25 eV as shown in Fig. 7. The DCl product is backward scattered at low energy. It becomes more sideways scattered as the collision energy rises, but remains predominantly in the backward hemisphere. Further, from Table X, it is clear that the umbrella mode of the product CD_3 is hardly excited at all. Thus, these calculated cross sections and differential cross sections are in excellent agreement with the experimental observations.[14,18]

TABLE IX. Calculated and experimental kinetic isotope effects for the reactions $Cl+CH_4 \rightleftharpoons HCl+CH_3$.

	$(Cl+CH_4)/(Cl+CD_4)$			$(HCl+CH_3)/(DCl+CD_3)$	
T/K	This work	Expt. (Ref. 41)	Expt. (Ref. 42)	This work	Calc. (Ref. 10)
200	23.9			2.7	3.5
250	12.4			2.5	3.3
300	7.7	10.9	12.2	2.3	3.1
350	5.3	7.4		2.1	2.9
400	3.9	5.2		1.9	2.7
450	3.1	3.9		1.7	2.5
600	1.8			1.3	2.1
800	1.2			1.0	

V. CONCLUSIONS

A three dimensional potential energy surface for the $Cl+CH_4 \rightleftharpoons HCl+CH_3$ reaction in C_{3V} symmetry has been

TABLE X. Relative cross sections $\sigma_{\nu_{3b}\nu_4 \rightarrow \nu\nu_2}/a_0^2$ for the reaction $Cl+CH_4(\nu_{3b},\nu_4) \rightarrow HCl(\nu)+CH_3(\nu_2)$ at a kinetic energy $E_{kin}=0.159$ eV, and for the reaction $Cl+CD_4(0,0) \rightarrow DCl(\nu)+CD_3(\nu_2)$ at a few kinetic energies.

$Cl+CH_4$			$Cl+CD_4$		
(ν_{3b},ν_4)	(ν,ν_2)	$\sigma_{\nu_{3b}\nu_4 \rightarrow \nu\nu_2}$	E_{kin}/eV	(ν,ν_2)	$\sigma_{00 \rightarrow \nu\nu_2}$
(0,0)	(0,0)	12.87	0.15	(0,0)	0.15
	(0,1)	0.02	0.18	(0,0)	3.70
				(0,1)	0.04
(1,0)	(0,0)	0.41			
	(0,1)	6.10	0.22	(0,0)	13.01
	(0,2)	1.57		(0,1)	0.11
	(0,3)	13.66			
	(0,4)	0.12	0.25	(0,0)	17.48
				(0,1)	0.23
	(1,0)	11.74		(0,2)	0.001
	(1,1)	2.11			

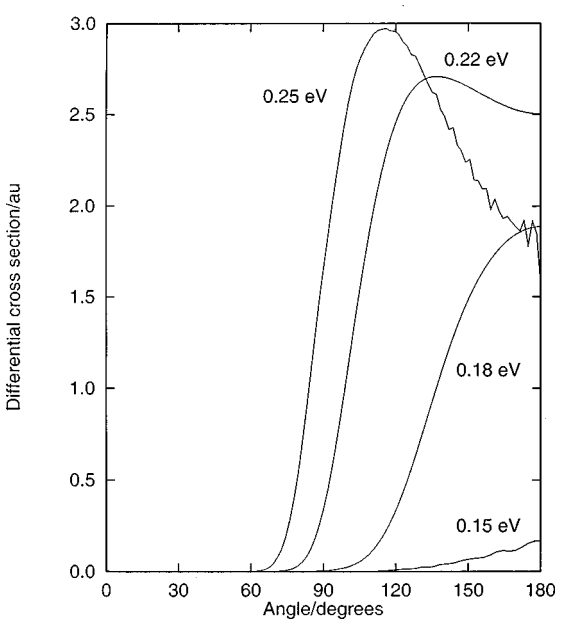

FIG. 7. Differential cross sections for the reaction $Cl+CD_4(0,0) \rightarrow DCl(0)+CH_3(0)$ at several kinetic energies. The angle $\theta_R=\pi$ refers to backward scattering of the DCl product.

calculated using a dual-level *ab initio* MP2/SAC theory with a well balanced MC-311G($2d,d,p$) basis set. An analytic potential energy function was obtained. This potential gives a classical barrier height of 6.96 kcal/mol for the forward reaction and an endoergicity of 5.40 kcal/mol. A correction is made to account for the zero-point energy of all modes not explicitly treated in the dynamics. The effective potential then obtained gives a vibrationally adiabatic ground-state barrier height and endothermicity (0 K) of 3.36 kcal/mol and 1.19 kcal/mol, respectively, for $Cl+CH_4$, and 4.42 kcal/mol and 2.29 kcal/mol, respectively, for $Cl+CD_4$. These values are in good agreement with experimental and previous theoretical results.

The rotating line umbrella model has been employed to perform the quantum dynamics studies of the $Cl+CH_4 \rightleftharpoons HCl+CH_3$ and $Cl+CD_4 \rightleftharpoons DCl+CD_3$ reactions. All calculated rate constants agree with measured results to within a factor two or better. It was found that the kinetic isotope effects ($Cl+CH_4/Cl+CD_4$) are larger and more temperature dependent than those of the reverse process ($HCl+CH_3/DCl+CD_3$). It is, however, expected that the presently obtained isotope effects are underestimated by roughly 30%.

Finally, differential cross sections for the $Cl+CD_4(0,0) \rightarrow DCl(0)+CD_3(0)$ reaction have been calculated at a few collision energies (0.15–0.25 eV). The results show that the CD_3 product is hardly excited at all and that the DCl product is dominantly backscattered. These results are in excellent agreement with recent experimental measurements.

ACKNOWLEDGMENTS

The calculations were carried out on a Silicon Graphics Power Challenge supercomputer and a cluster of workstations at Chalmers University of Technology and Göteborg University. This research has been supported by the Swedish Natural Science Research Council (NFR), the Swedish Council for Planning and Coordination of Research (FRN) and the Wallenberg Foundation.

[1] R. Atkinson, D.L. Baulch, R.A. Cox, R.F. Hampson, Jr., J.A. Kerr, and J. Troe, J. Phys. Chem. Ref. Data **21**, 1125 (1992).
[2] T.N. Truong, D.G. Truhlar, K.K. Baldridge, M.S. Gordon, and R. Stecker, J. Chem. Phys. **90**, 7137 (1989).
[3] K.D. Dobbs and D.A. Dixon, J. Phys. Chem. **98**, 12584 (1994).
[4] W.T. Duncan and T.N. Truong, J. Chem. Phys. **103**, 9642 (1995); **109**, 3703(E) (1998).
[5] J. Espinosa-García and J.C. Corchado, J. Chem. Phys. **105**, 3517 (1996).
[6] O. Roberto-Neto, E.L. Coitiño, and D.G. Truhlar, J. Phys. Chem. **A102**, 4568 (1998).
[7] J.S. Pilgrim, A. McIlory, and C.A. Taatjes, J. Phys. Chem. **A101**, 1873 (1997).
[8] W.B. DeMore, S.P. Sander, D.M. Golden, R.F. Hampson, M.J. Kurylo, C.J. Howard, A.R. Ravishankara, C.E. Kolb, and M.J. Molina, JPL publications 92-20, Jet Propulsion Laboratory, 1992.
[9] Y. Chen, E. Tschuikow-Roux, and A. Rauk, J. Phys. Chem. **95**, 9832 (1991).
[10] Y. Chen, A. Rauk, and E. Tschuikow-Roux, J. Phys. Chem. **95**, 9900 (1991).
[11] G. Nyman, H.G. Yu, and R.B. Walker, J. Chem. Phys. **109**, 5896 (1998).
[12] H.G. Yu and G. Nyman, Phys. Chem. Chem. Phys. **1**, 1181 (1999).
[13] H.G. Yu and G. Nyman, J. Chem. Phys. **110**, 7233 (1999).
[14] W.R. Simpson, T.P. Rakitzis, S.A. Kandel, T. Lev-On, and R.N. Zare, J. Phys. Chem. **100**, 7938 (1996).
[15] W.R. Simpson, A.J. Orr-Ewing, and R.N. Zare, Chem. Phys. Lett. **212**, 163 (1993).
[16] W.R. Simpson, T.P. Rakitzis, S.A. Kandel, A.J. Orr-Ewing, and R.N. Zare, J. Chem. Phys. **103**, 7313 (1995).
[17] A.J. Orr-Ewing, W.R. Simpson, T.P. Rakitzis, S.A. Kandel, and R.N. Zare, J. Chem. Phys. **106**, 5961 (1997).
[18] S.A. Kandel and R.N. Zare, J. Chem. Phys. **109**, 9719 (1998).
[19] M.S. Gordon and D.G. Truhlar, J. Am. Chem. Soc. **108**, 5412 (1986).
[20] M.S. Gordon and D.G. Truhlar, Int. J. Quantum Chem. **31**, 81 (1987).
[21] M.S. Gordon, K.A. Nguyen, and D.G. Truhlar, J. Phys. Chem. **93**, 7356 (1989).
[22] R. Krishnan, J.S. Binkley, R. Seeger, and J.A. Pople, J. Chem. Phys. **72**, 650 (1980).
[23] A.D. McLean and G.S. Chandler, J. Chem. Phys. **72**, 5639 (1980).
[24] M.J. Frisch, G.W. Trucks, H.B. Schlegel, P.M.W. Gill, B.G. Johnson, M.A. Robb, J.R. Cheeseman, T. Keith, G.A. Petersson, J.A. Montgomery, K. Raghavachari, M.A. Al-Laham, V.G. Zakrzewski, J.V. Ortiz, J.B. Foresman, J. Cioslowski, B.B. Stefanov, A. Nanayakkara, M. Challacombe, C.Y. Peng, P.Y. Ayala, W. Chen, M.W. Wong, J.L. Andres, E.S. Replogle, R. Gomperts, R.L. Martin, D.J. Fox, J.S. Binkley, D.J. Defrees, J. Baker, J.P. Stewart, M. Head-Gordon, C. Gonzalez, and J.A. Pople, GAUSSIAN 94, Revision E.2 (Gaussian, Inc., Pittsburgh, 1995).
[25] J.N. Murrell, S. Carter, S.C. Farantos, P. Huxley, and A.J.C. Varandas, *Molecular Potential Energy Functions* (Wiley, Chichester, 1984).
[26] A.J.C. Varandas, in *Structure and Dynamics of Weakly Bound Molecular Complexes*, edited by A. Weber (D. Reidel, Dordrecht, 1987), p. 357.
[27] H.G. Yu and G. Nyman, Chem. Phys. Lett. **298**, 27 (1998).
[28] D.E. Manolopoulos, J. Chem. Phys. **85**, 6425 (1986).
[29] D.E. Manolopoulos, M. D'Mello, and R.E. Wyatt, J. Chem. Phys. **91**, 6096 (1989).
[30] G. Nyman and D.C. Clary, J. Chem. Phys. **99**, 7774 (1993).
[31] G. Nyman and D.C. Clary, J. Chem. Phys. **101**, 5756 (1994).
[32] U. Manthe, T. Seideman, and W.H. Miller, J. Chem. Phys. **99**, 10078 (1993).
[33] J.M. Bowman, J. Phys. Chem. **95**, 4960 (1991).
[34] G. Nyman, J. Chem. Phys. **104**, 6154 (1996).
[35] H.G. Yu and G. Nyman, J. Chem. Phys. **111**, 3508 (1999).
[36] K.P. Huber and G. Herzberg, *Molecular Spectra and Molecular Structure. IV. Constant of Diatomic Molecules* (Van Nostrand, New York, 1979).

[37] *JANAF Thermochemical Tables*, edited by M.W. Chase, Jr. *et al.* (Natl. Standard Ref. Data Ser. Natl. Bur. Stand., Washington, DC, 1985).
[38] J.J. Russel, J.A. Seetula, S.M. Senkan, and D. Gutman, Int. J. Chem. Kinet. **20**, 759 (1988).
[39] M.S. Zahniser, B.M. Berquist, and F. Kaufman, Int. J. Chem. Kinet. **10**, 15 (1978).
[40] M.-L. Pohjonen and J. Koskikallio, Acta Chem. Scand. **A33**, 449 (1979).
[41] G. Chiltz, R. Eckling, P. Goldfinger, G. Huybrechts, H.S. Johnston, L. Meyers, and G. Verbeke, J. Chem. Phys. **5**, 1053 (1963).
[42] Y. Matsumi, K. Izumi, V. Skorokdov, M. Kawasaki, and N. Tanaka, J. Phys. Chem. A **101**, 1216 (1977).